Micromagnetic simulations of magnetization dynamics in a nanowire induced by a spin-polarized current injected via a point contact

D. V. Berkov
Innovent Technology Development, Pruessingstraße 27B, D-07745 Jena, Germany

C. T. Boone and I. N. Krivorotov
Department of Physics and Astronomy, University of California, Irvine, CA 92697-4575, USA

(Received 19 October 2010; published 22 February 2011)

We present a detailed numerical analysis of the magnetization auto-oscillations induced in a thin NiFe nanowire by a direct spin-polarized current injected via a square-shaped CoFe nanomagnet [a system experimentally studied in Boone *et al.* Phys. Rev. B **79**, 140404 (2009).]. We demonstrate that all auto-oscillation modes in the nanowire are localized under the nanocontact for magnetic field applied in the plane of the nanowire. This mode localization is induced by a strong, stray magnetic field acting on the NiFe nanowire from the CoFe current injector. We find that the auto-oscillation frequency, power, and the frequency shift with the current strongly depend on the exchange constant of NiFe. We also find that the auto-oscillation power depends nonmonotonically on the CoFe saturation magnetization, and we demonstrate that this effect has its origin in resonant excitation of the CoFe eigenmodes by magnetization oscillations in the NiFe nanowire. The calculated dependence of the oscillation frequency on current is in good agreement with the experiment. However, the agreement between theory and experiment for the oscillation power is unsatisfactory. Finally, we have shown that an auto-oscillatory mode propagating along the nanowire in the system under study is possible when a sufficiently strong out-of-plane field is applied.

DOI: 10.1103/PhysRevB.83.054420 PACS number(s): 85.75.−d, 05.40.−a, 75.75.−c

I. INTRODUCTION

Spin torque (ST) from spin-polarized current applied to a metallic ferromagnet[1–4] can induce steady-state oscillations of this magnetization and thereby generate a microwave signal.[5–7] The frequency of the microwave signal is tunable by the direct current bias, and thus such nanostructures function as microwave voltage-controlled oscillators of nanoscale dimensions. Practical applications of spin torque nano-oscillators (STNOs) require high output power levels and low phase noise.[8–10] Several approaches pursuing these goals, such as phase locking of arrays of STNOs[11–14] and development of STNOs based on magnetic tunnel junctions,[15–18] are active areas of research.

STNOs also form a peculiar class of nonlinear dynamical systems. The nonlinearity of a STNO (the dependence of its frequency on power) can be tuned from nearly zero to very large values by changing the direction and magnitude of the external magnetic field.[19,20] For many STNO geometries, the nonlinearity reaches values far exceeding[19,21–24] those observed in other auto-oscillatory systems. Owing to their nanoscale dimensions, the magnetic energy of STNOs is comparable to the ambient temperature and thus the STNO dynamics are strongly affected by random thermal torques.[25,26] Therefore STNOs provide a unique testing ground for studies of stochastic auto-oscillatory systems in the strongly nonlinear regime.

To date, two major STNO geometries have been studied: (i) spin valve nanopillars in which propagation of magnetic excitations is restricted by the ferromagnet boundaries in all three spatial dimensions (zero-dimensional systems, 0D),[5,27,28] and (ii) point contacts to spin valves, in which magnetic excitations can propagate in the plane of the spin valve (two-dimensional systems, 2D).[6,8,11,12,29] The two-dimensional systems offer the advantage of phase locking of nearby STNOs via interaction by spin waves propagating in the common ferromagnetic free layer.[11,12] The phase locking regime is attractive from the practical point of view because the output power of STNOs increases and their phase noise decreases in this regime.[11–13]

Another recently studied SNTO system is a nanowire spin valve with a point-contact for spin-polarized current injection.[30] In this system, schematically shown in Fig. 1, magnetic excitations can, in principle, propagate only in the direction parallel to the nanowire axis. This one-dimensional (1D) STNO system can potentially improve the phase locking properties of SNTO arrays compared to the 2D point-contact systems. Indeed, in 2D systems, the coupling between neighboring oscillators is weakened by the $1/R$ geometric decay of the amplitude of spin waves mediating the coupling (R is the distance between the neighboring STNOs). In this paper, we numerically study auto-oscillations of magnetization in such 1D STNO systems. We examine the factors that determine the 1D STNO performance and discuss pathways to practical realization of phase-locked 1D STNO arrays.

II. EXPERIMENTAL SETUP

Figure 1 schematically shows the structure of the 1D nanowire STNO experimentally studied in Ref. 30. In this work, we make micromagnetic simulations of magnetization dynamics in this nanowire STNO using the exact geometry and the material parameters of the experimentally studied system.[30] The free layer of this 1D STNO is a 6-nm-thick, 50-nm-wide Permalloy (Py $\equiv Ni_{86}Fe_{14}$) nanowire lithographically defined on top of a Cu/Ta multilayer that serves as the bottom electrical lead. Spin-polarized current is injected into the nanowire through a 50×50 nm^2 $Co_{50}Fe_{50}$ (15 nm)/Cu (8 nm) bilayer patterned on top of the Py nanowire. The top Au/Ta

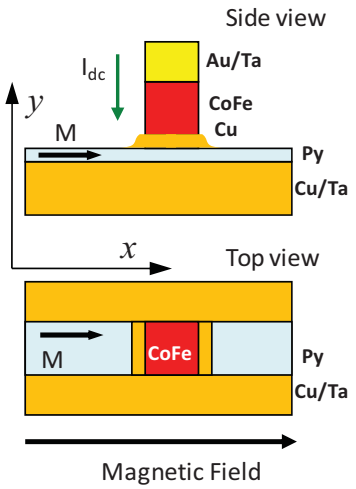

FIG. 1. (Color online) Schematic of the 1D STNO device (side and top views). The free layer of this STNO is a Py nanowire and the fixed layer is a square $Co_{50}Fe_{50}$ nanomagnet.

bilayer lead is connected to the $Co_{50}Fe_{50}$ nanomagnet, and spin-polarized current is injected from the $Co_{50}Fe_{50}$ polarizer into the Py nanowire by applying direct current between the top and the bottom leads. The value of saturation magnetization of the Py ($M_{Py} = 580$ emu/cm^3) film was measured by vibrating sample magnetometry.

Persistent auto-oscillations of magnetization in the Py nanowire are excited by applying a direct current I_{dc} between the top and bottom leads of the device with electrons moving from Py to $Co_{50}Fe_{50}$. These GHz-range auto-oscillations of magnetization give rise to resistance oscillations due to the giant magnetoresistance effect (GMR). As a result, a microwave voltage is generated by the current-biased STNO device.[5] In the experiment, this microwave voltage is amplified and its power spectrum is measured using a microwave spectrum analyzer.[5]

III. NUMERICAL SIMULATIONS METHOD AND STATIC HYSTERESIS LOOPS

A. Simulation details

Numerical simulation have been carried out using the MicroMagus software package[31] supplemented by a special routine allowing the introduction of a site-dependent damping in order to avoid the spin-wave reflections from the wire ends.[37] Both the Py nanowire and CoFe square nanomagnet were included in the simulated system and discretized in-plane using lateral cell sizes 3.125 × 3.125 nm^2, so that, e.g., the CoFe square was subdivided in-plane into 16 × 16 cells. Test runs have shown that finer discretization did not lead to noticeable changes in the simulated power spectra and that no discretization of Py and CoFe layers perpendicular to the sample plane was necessary. We employ a Cartesian coordinate system, in which the x axis lies in the sample plane parallel to the nanowire, the y axis is perpendicular to the sample plane and the z axis is in the sample plane perpendicular to the nanowire. the y axis, perpendicular to the film plane, so that the z axis is directed in-plane perpendicular to the long nanowire axis.

For quasistatic simulations of hysteresis loops, we start from the saturated state in a large external field $H_{ext}^{max} =$ 2000 Oe directed nearly parallel to the x axis (we have introduced a small angle of 2° between the field direction and the nanowire axis to avoid artificial degeneracies arising in simulations when H_{ext} is exactly parallel to the x axis). Then we decrease the field in small steps to the negative saturation $H_{ext}^{min} = -2000$ Oe to obtain the decreasing-field loop branch. Then we increase the field to the initial value to check that the hysteresis loop is centrally symmetric with respect to the (M_x, H_x)-coordinate origin. GMR curves $\Delta R(H_x)$ shown in Fig. 2(b) were calculated from equilibrium magnetization states in a standard way, assuming that (i) the current density (current flows perpendicular to the layer planes) is homogeneous across the CoFe nanomagnet, (ii) the vertical cell stacks (CoFe/Py cell pairs along the y direction) are connected as parallel resistors, and (iii) the magnetoresistance change of such a vertical stack depends on the angle θ between the magnetizations of CoFe and Py stack cells as[30] $\Delta R(\theta) = \Delta R_{max} \cdot \sin^2(\theta/2)/[1+\chi \cos^2(\theta/2)]$. The value of the magnetoresistance asymmetry parameter χ was set to $\chi = 1$ as determined in Ref. 30.

To perform dynamic simulations at a fixed external field, we first find the equilibrium magnetization state in this field ($H_x = 500$ Oe used in the experiment)[30] and then turn on the direct current I to obtain the dependences of the oscillation frequency $f(I)$ and power $p(I)$ on the current. For the spin torque we use the standard Slonczewski term as in our previous publications.[37,39] The spin torque magnitude is proportional to $P \cdot I$, where P is the degree of spin polarization of the electrical current. We plot all current-dependent quantities as functions of the reduced current I/I_{cr}, with I_{cr} being the auto-oscillation onset current (the lower critical current). Comparing the value I_{cr} obtained in simulations with the corresponding experimental value, we can extract the degree of current polarization P. In our simulations, spin torque was assumed to act only on the Py magnetization directly under the CoFe nanomagnet. The direction of the spin polarization acting on the Py magnetization was dynamically adjusted to the local direction of the CoFe magnetization, which was time dependent due to the magnetodipolar interaction between the Py and CoFe layers.

We have also verified that spin torque[32] acting on the CoFe magnetization from the Py layer did not have a significant effect on the dynamics of the system. This torque can be neglected due to much larger values of the saturation magnetization and the thickness of the CoFe nanomagnet compared to the Py nanowire.

The Oersted field was neglected in our simulations because for the typical currents used in the experiment, ∼2 mA, and the lateral CoFe nanomagnet dimensions, 50 × 50 nm^2, its maximum value is $H_{Oe}^{max} \approx 130$ Oe (for this estimate, we assumed that the Oersted field is produced by a current in an infinitely long wire with the 50 × 50 nm^2 square cross section). This maximal value is already significantly smaller than the applied field value of 500 Oe, and the Oersted field magnitude averaged over the CoFe cross section is even smaller. Furthermore, in the experiment, the magnetic multilayer stack height is of the same order of magnitude as the CoFe lateral dimensions and thus the infinite wire

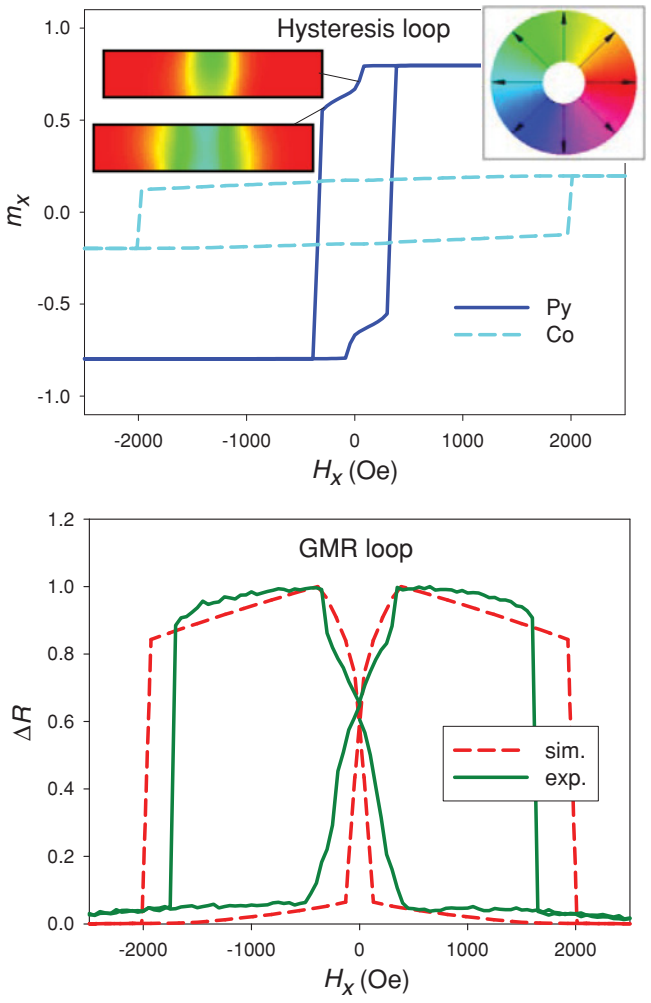

FIG. 2. (Color online) Magnetization (upper panel with the color wheel representing the magnetization direction) and magnetoresistance (lower panel) hysteresis loops of the studied system calculated for $M_{Py} = 580$ emu/cm^3, $A_{Py} = 1 \times 10^{-6}$ erg/cm, $M_{CoFe} = 1800$ emu/cm^3, and $A_{CoFe} = 3 \times 10^{-6}$ erg/cm.

approximation significantly overestimates the Oersted field magnitude.

B. Results of quasistatic simulations

We simulated the quasistatic hysteresis behavior of our system and compared it to the experimentally measured magnetoresistance loops (see Fig. 1 in Ref. 30). In our quasistatic simulations we used the experimental system geometry: $Ni_{86}Fe_{14}$ (Py) nanowire with width $w = 50$ nm, thickness $h_{Py} = 6$ nm separated by the Cu layer with thickness $h_{Cu} = 8$ nm from the $Co_{50}Fe_{50}$ square nanomagnet with the lateral dimensions 50×50 nm^2 and thickness $h_{CoFe} = 15$ nm. For magnetic parameters we employed the experimentally measured value of the Py magnetization $M_{Py} = 580$ emu/cm^3 and the standard parameter values for the $Co_{50}Fe_{50}$ alloy: $M_{CoFe} = 1800$ emu/cm^3 and $A_{CoFe} = 3 \times 10^{-6}$ erg/cm. Since the value of the exchange constant A_{Py} for ultrathin $Ni_{86}Fe_{14}$ is not known, we performed simulations for a number of values of A_{Py} smaller than the bulk Py exchange constant [$A_{Py} = (1–1.3) \times 10^{-6}$ erg/cm].

We have also taken into account the random magnetocrystalline anisotropy present both in Py and CoFe layers. For this purpose we have used the ability of the MicroMagus package to create random grain structures and to assign to each crystal grain its own set of the anisotropy axes. We have assumed that the average grain size in both magnetic layers is $\langle D \rangle = 10$ nm. A cubic magnetocrystalline anisotropy was assigned to grains of both Py and CoFe, with the standard anisotropy constant $K_{Py} = 5 \times 10^3$ erg/cm^3 for Py and $K_{CoFe} = -2 \times 10^5$ erg/cm^3 for $Co_{50}Fe_{50}$ (see Ref. 42). Anisotropy axes were oriented randomly for different grains. Due to the self-averaging of the random anisotropy contributions for systems with small crystallites and randomly oriented anisotropy axes we have found that the contribution of the anisotropy field to the magnetization dynamics is negligible, i.e., oscillation frequencies and powers for systems with different realizations of crystal grain anisotropy axes directions did not demonstrate any significant differences.

In principle, thin ferromagnetic layers may also exhibit some surface anisotropy. However, lacking the exact information concerning this anisotropy of magnetic layers used in our study, we have set the surface anisotropy constants of both magnetic layers to zero.

Simulation results for our system are presented in Figs. 2 and 3 together with the magnetoresistance loop measured experimentally. Comparison of the simulated magnetization and GMR loops shown Fig. 2 reveals that the continuous resistance increase with decreasing field is due to formation of a 90° domain in the region of the Py nanowire directly under the CoFe nanomagnet. This domain formation under the CoFe nanomagnet is assisted by the large stray field of the CoFe nanomagnet. For $A_{Py} = 1 \times 10^{-6}$ erg/cm, this domain appears at $H_x \approx 50$ Oe and rapidly expands [see magnetization color maps in Fig. 2(a)] leading to the complete magnetization reversal of the Py nanowire at $H_x \approx -400$ Oe. At this field, resistance reaches its maximal value and remains approximately constant until the abrupt magnetization reversal of the CoFe nanoelement occurs at $H_x \approx -2000$ Oe. We also note that the magnetization state of the CoFe nanomagnet in positive fields is the so-called C state, so that its stray field acting on the Py nanowire is strongly asymmetric with respect to the long nanowire axis. This stray field asymmetry is important for understanding of the dynamic mode localization pattern discussed in Sec. IV.

Comparison of the experimental and simulated magnetoresistance loops (lower panel in Fig. 2) shows that for the assumed standard Py exchange stiffness $A_{Py} = 1 \times 10^{-6}$ erg/cm the simulated GMR loop is only qualitatively similar to the experimentally measured loop. To achieve better agreement with the experimental MR loop, we use the poorly known exchange stiffness of the thin Py film, A_{Py}, as a fitting parameter. We performed simulations for $A_{Py} = 0.8 \times 10^{-6}$, 0.7×10^{-6}, and 0.6×10^{-6} erg/cm. The results are shown in Fig. 3, which illustrates that smaller A_{Py} indeed leads to a better agreement with the measured GMR loop. For smaller values of A_{Py}, the nucleation field of the central 90° domain in Py increases with decreasing A_{Py}, leading to a more gradual resistance increase near zero field, in agreement with the experiment. We also note that the discrepancy between simulated and measured CoFe switching

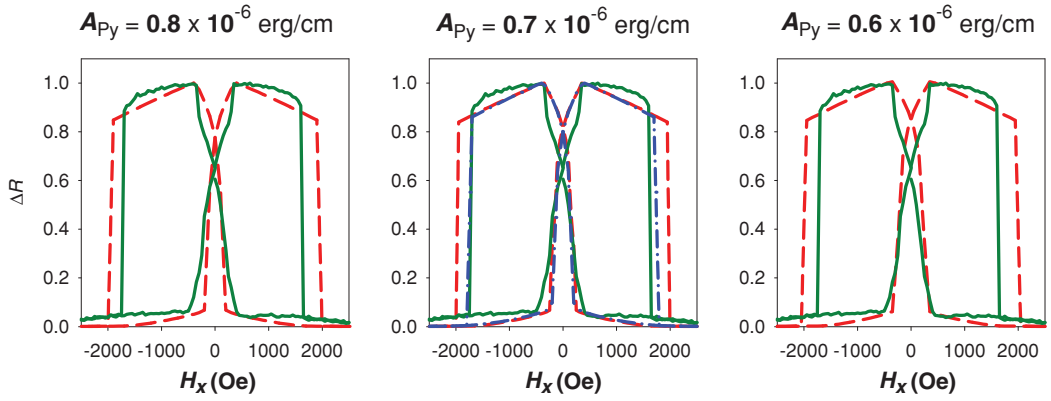

FIG. 3. (Color online) Magnetoresistance loops for $M_{Py} = 580$ emu/cm^3, $M_{CoFe} = 1800$ emu/cm^3, $A_{CoFe} = 3 \times 10^{-6}$ erg/cm, and three values of Py exchange stiffness constants A_{Py} (solid lines: experiment; dashed lines: simulations). Smaller values of the Py exchange constant significantly improve the agreement with the experiment for the inner part of the magnetoresistance loop corresponding to the Py layer reversal. The dash-dotted blue line for $A_{Py} = 0.7 \times 10^{-6}$ erg/cm (central panel) shows that the CoFe switching field can be reduced to the measured value by introducing a small edge roughness at the CoFe edges (see text for details).

fields is eliminated if a small CoFe edge roughness is taken into account. This roughness was simulated as a magnetization decrease of the outmost rows of the CoFe discretization cells, in which normalized magnetization was changed randomly in the interval [0.5–1.0]. Figure 3(b) shows that this procedure leads to a perfect agreement for CoFe switching fields for $A_{Py} = 0.7 \times 10^{-6}$ erg/cm.

IV. SIMULATED SYSTEM DYNAMICS AND COMPARISON WITH EXPERIMENTAL FINDINGS

Since the Oersted field is neglected in our simulations, the current I and the current spin polarization P enter the theoretical description of current-induced magnetization dynamics only as the product $I \cdot P$. For this reason we calculate all current-dependent quantities as functions of reduced current I/I_{cr}, where I_{cr} is the critical current for the onset of magnetization auto-oscillations. The value of the current polarization P can be calculated by setting the simulated critical current equal to the experimental value. All results presented in this section are calculated for a static applied field $H_x = 500$ Oe (along the nanowire axis). Thermal fluctuations of magnetization are not included in our simulations.

A. General features of the magnetization oscillations

For the geometry under study (see Fig. 1) and all sets of magnetic parameters used in our simulations, the ST-induced magnetization dynamics exhibits the following general features:

(1) There are two qualitatively different auto-oscillation regimes: low and high current regimes.

(2) The *low current regime* starts at the onset current I_{cr} and persists to $I/I_{cr} \approx 3$–5. In this regime, the magnetizations of both Py and CoFe layers precess approximately around the external field direction and magnetization oscillations are highly phase coherent. The power spectrum exhibits spectral peaks with a width smaller than our spectral resolution (~10 MHz), which is limited by the simulation time.

(3) In the Py nanowire, the coherent oscillations of magnetization are always localized within the area under the CoFe nanomagnet (see spatial power maps in Fig. 6). This localization is due to the strong inhomogeneity of the CoFe stray field acting on the Py wire. In this sense, our system differs qualitatively from extended multilayer devices employing the point-contact current injection,[8] where the localization of the ST-induced oscillations is caused by the strong nonlinearity of the auto-oscillation modes (e.g., bullet,[33] vortex,[34] or vortex-antivortex pairs[35–37]). In our case, magnetization oscillations in the linear regime are already localized within the Py nanowire area under the CoFe nanomagnet due to the stray field from the CoFe nanomagnet. Analogous localization of thermal spin waves was observed in patterned nanoelement arrays.[38]

(4) At a relatively high current I_{sw}, the system switches to a qualitatively different magnetization state. In the zero-current (equilibrium) state, the CoFe nanomagnet magnetization is in the so-called C state and the CoFe stray field causes only a small deviation of the Py layer magnetization from the uniform state [Fig. 4(a)]. For $I > I_{sw}$, the CoFe magnetization jumps into an S state, and its stray field leads to a large-angle rotation of the Py magnetization directly under the CoFe nanomagnet. As the result of this process, magnetizations of CoFe and Py are directed approximately *perpendicular* to each other. If after this magnetization jump we turn the spin current off, the system magnetization remains trapped in the state shown in Fig. 4(b), which we shall call the 90° state. ST-induced oscillations in this regime (present if we do not switch the current off) are quasichaotic, have a much lower power and broad spectral lines, and thus they cannot be detected experimentally. For this reason, in what follows we concentrate on the coherent low-current regime.

B. Effect of the Py exchange constant A_{Py}

The exchange constant A_{Py} of our thin $Ni_{86}Fe_{14}$ film is not well known, and its relatively low saturation magnetization $M_S = 580$ Oe indicates that its exchange stiffness may be

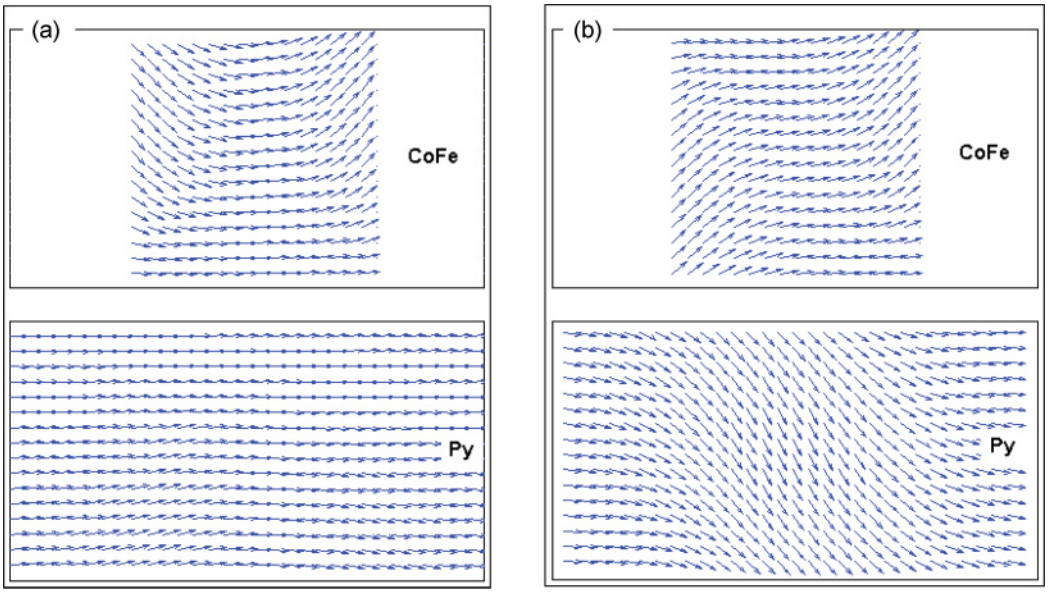

FIG. 4. (Color online) Equilibrium magnetization configurations of Py and CoFe layers in the external field $H_x = 500$ Oe at zero current (a) and after switching in the high-current regime (b). To compute the static equilibrium state (b), spin torque was turned off after the magnetization switching.

significantly lower than the "standard" value for bulk Py [which is usually reported within the interval (1–1.3) $\times$ 10^{-6} erg/cm]. For this reason, we first studied the dependence of the system dynamics on the $Ni_{86}Fe_{14}$ exchange constant. The results of this study are summarized in Fig. 5, which shows the dependences of the simulated auto-oscillation frequency and power on the reduced current I/I_{cr} for several values of A_{Py}, along with the experimental results.[30]

As a general trend, we observe that smaller exchange stiffness leads to lower oscillation frequencies, as shown in Fig. 5(a). This is a natural consequence of the localization of oscillations under the CoFe nanomagnet (see maps displaying the spatial distribution of the oscillation power in Fig. 6). The frequency of such a localized mode is largely determined by the exchange stiffness of the magnetic material and hence the frequency decreases with decreasing exchange constant. We note that the dependence of the oscillation frequency on the Py exchange constant is quite strong. This feature can be used, in principle, for measurements of the exchange constant in ultrathin films by comparing the calculated $f(I)$ curves for different values of A with the experimental data. Figure 5(a) shows that the best agreement between the simulated and the measured frequencies is found for $A_{Py} = (0.6–0.65) \times 10^{-6}$ erg/cm. This result is in agreement with the value of A_{Py} obtained from our quasistatic magnetoresistance loop simulations (Fig. 3).

As we already discussed, oscillatory modes in our system are localized within the region of the Py nanowire directly under the CoFe nanomagnet because the stray field of the CoFe nanomagnet field in this region is directed roughly opposite to the external field. This situation is fully analogous to the localization of edge modes in patterned nanoelements,[38] where the self-demagnetizing field of the nanoelement is directed opposite to the external field, creating a potential well for the magnetization oscillations. An important distinct feature of our system is the strong asymmetry of the CoFe stray field with respect to the nanowire axis [resulting from the C state of CoFe magnetization; see Fig. 4(a)] acting on the Py nanowire. This asymmetry results in the corresponding asymmetry of the

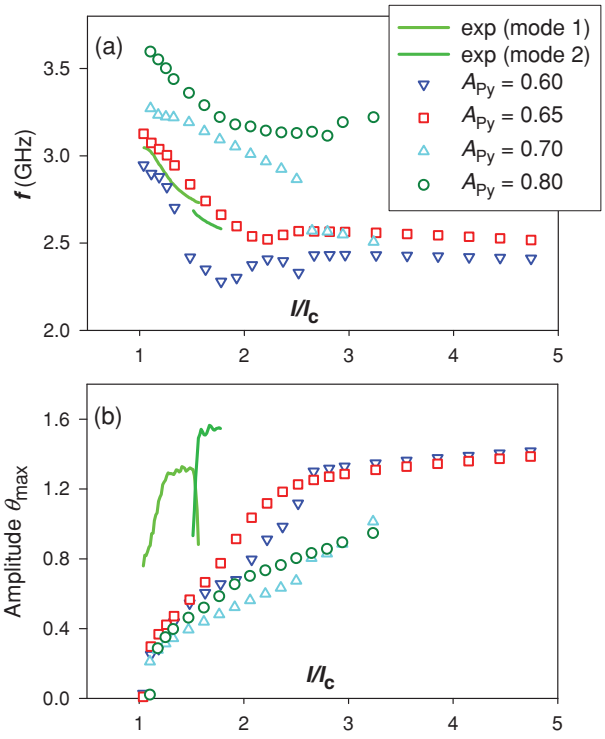

FIG. 5. (Color online) Effect of the Py exchange constant A_{Py} on the dependences of the oscillation frequency (a) and average oscillation amplitude (b) on the reduced current I/I_c (for $M_{CoFe} = 1800$ emu/cm^3). The solid lines in both panels show the experimental data from Ref. 30.

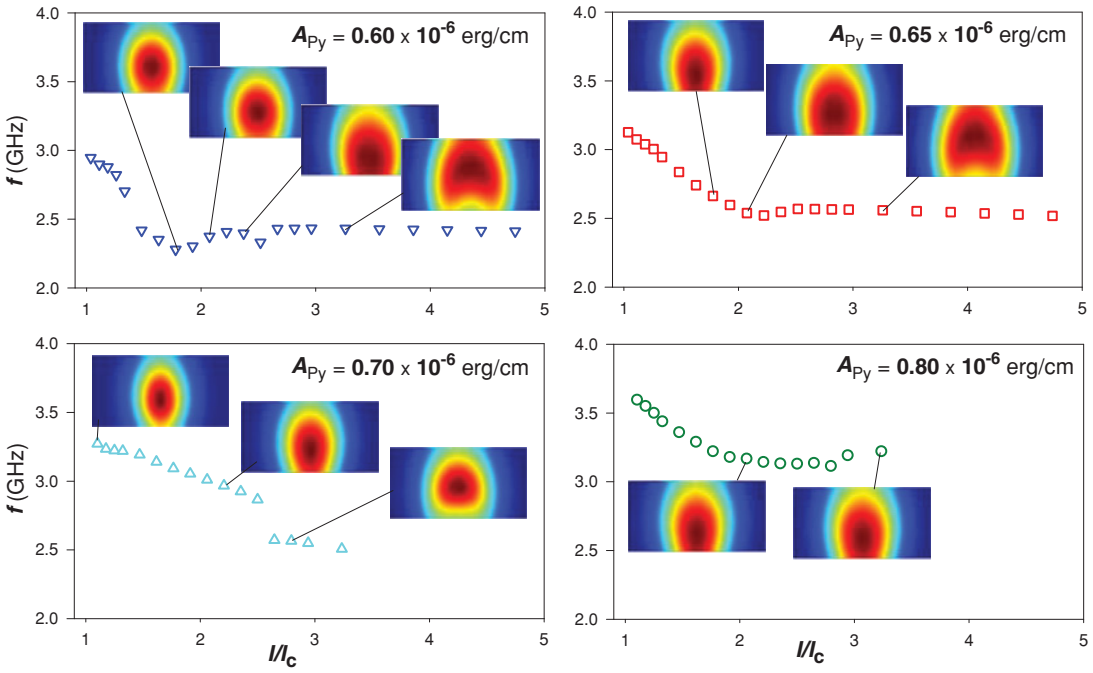

FIG. 6. (Color online) Power (defined as the mean-square value of the m_z component) spatial distribution maps of the auto-oscillatory modes as a function of direct current. The area shown on all color maps corresponds to the physical size 100 × 50 nm^2, so that all modes are localized within the Py nanowire region under the CoFe square.

mode localization pattern clearly seen in spatial power maps shown in Fig. 6.

For some values of the Py exchange constants, e.g., $A_{Py} = 0.6 \times 10^{-6}$ and 0.7×10^{-6} erg/cm, we observe frequency jumps in the dependence of frequency on current as shown in Fig. 6. As discussed in our previous work,[39] these jumps are caused by the transitions between modes with different spatial localization patterns. However, the mode localization pattern may change without leading to an appreciable frequency jump. This means that the change of the mode localization type is a necessary, but not sufficient, condition to produce a jump in the dependence of frequency on current.

C. Effect of the CoFe magnetization M_{CoFe}

Another important magnetic parameter affecting the current-induced dynamics is the saturation magnetization M_{CoFe} of the CoFe alloy. For this reason we also studied the influence of this parameter on the system magnetization dynamics, changing M_{CoFe} in the interval 1600–1800 emu/cm^3, which is a relevant range for CoFe alloys. Our simulations demonstrate that the increase of M_{CoFe} leads to a decrease of the small-amplitude Py oscillation frequency (frequency at the critical current for the onset of auto-oscillations), as shown in Fig. 7(a). This effect is due to the increase of the CoFe stray field on the Py wire with increasing M_{CoFe}.

The most striking effect of varying M_{CoFe} is the strong and *nonmonotonic* dependence of the oscillation power p, defined as the mean-square value of the m_z component, on M_{CoFe} [see the inset in Fig. 7(b)]. The sharp nonmonotonic dependence of the oscillation power on the CoFe magnetization suggests that this is a resonant effect. A possible reason for the nonmonotonic dependence $p(M_{CoFe})$ is resonant excitation of oscillations of the CoFe magnetization through *dynamic* magnetodipolar coupling to the ST-induced oscillations of the Py magnetization. To test this hypothesis, we performed numerical simulations of the small-amplitude magnetization dynamics of our system induced by a short field pulse. Fourier analysis of the magnetization oscillations occurring after such a pulse allows us fast and accurate determination of the eigenmode oscillation frequencies of the system under study. The dependence of the oscillation frequency of two low-frequency eigenmodes of the CoFe nanomagnet on M_{CoFe} obtained from such simulations is shown in Fig. 8 together with the frequency of the ST-induced auto-oscillations. This figure demonstrates that a strong coupling between the ST-induced m_x oscillations of Py and one of the edge modes of the CoFe nanomagnet is expected due to the frequency coincidence of these two types of oscillations. Figure 7 demonstrates that the value of $M_{CoFe} =$ 1700–1725 emu/cm^3 gives rise to this frequency coincidence condition and the power of ST-induced Py oscillations shows a minimum. For this resonance condition, the energy supplied to the system by the dc current is efficiently transferred to the CoFe oscillations, which decreases the amplitude of Py magnetization oscillations.

Another interesting feature of the magnetization dynamics for our system is the initial blue shift of the frequency with current for $M_{CoFe} =$ 1650 and 1700 emu/cm^3, because red frequency shift is usually expected for the in-plane precession mode of magnetization excited in our system.[40] The observed blue shift is most probably due to the strong localization of the oscillations in the potential well created by the CoFe stray

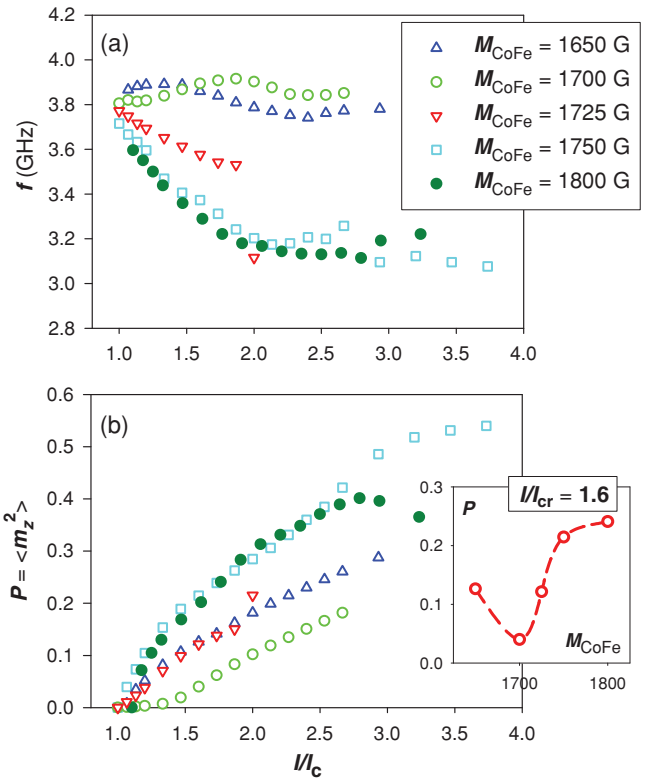

FIG. 7. (Color online) Effect of the CoFe magnetization M_{CoFe} (for $A_{\mathrm{Py}} = 0.8 \times 10^{-6}$ erg/cm) on the oscillation frequency (a) and oscillation power (b) defined as the mean-square value of the m_z component. The inset in (b) shows the nonmonotonic dependence of the oscillation power on M_{CoFe}.

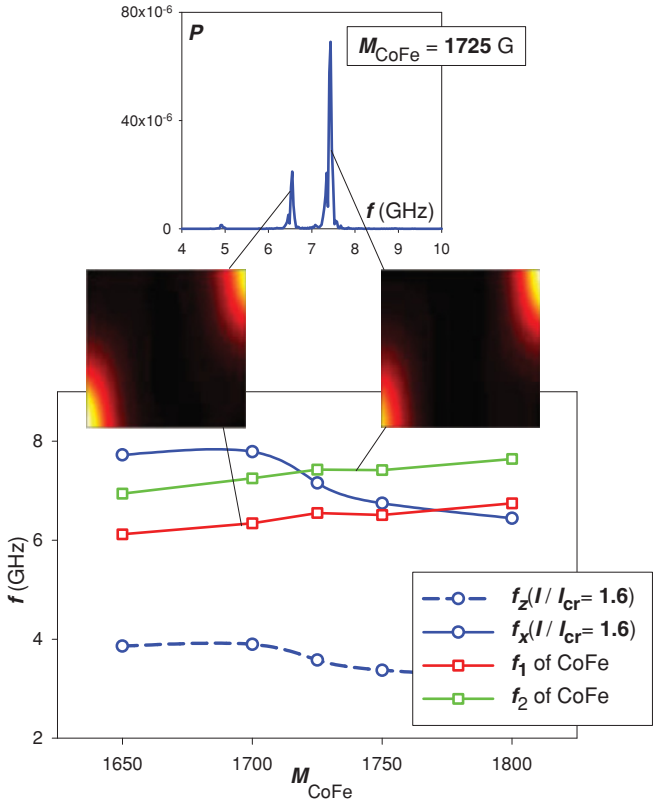

FIG. 8. (Color online) Frequencies of two low-energy eigenmodes of the CoFe nanomagnet (open squares) and frequency of ST-induced auto-oscillations (open circles) as functions of the CoFe magnetization M_{CoFe}. The upper panel shows the power spectrum of small-amplitude oscillations of magnetization of the CoFe nanomagnet induced by a sharp magnetic-field pulse. Color maps display the spatial distribution of the oscillation power of the CoFe eigenmodes. The two modes are distinguished by the phase relation and by the relation of the oscillation amplitudes between the opposite corners.

field. For currents above the critical current in the nonlinear dynamics regime, the auto-oscillatory mode excited in Py nanowire becomes more localized with increasing current and the exchange stiffness shifts the frequency to a higher value.

D. Comparison with experiment

Dependence of the auto-oscillation frequency on current. Figure 5(a) shows that our simulations are in a good agreement with the measured[30] dependence of frequency on current for A_{Py} between 0.6×10^{-6} erg/cm and 0.65×10^{-6} erg/cm (and $A_{\mathrm{CoFe}} = 3 \times 10^{-6}$ erg/cm, $M_{\mathrm{CoFe}} = 1800$ emu/cm^3). The relatively low value of the Py exchange stiffness required to achieve this agreement is not surprising,[41] considering that the saturation magnetization of the alloy used in the real device is also low ($M_{\mathrm{Py}} = 580$ emu/cm^3). Here we also note that the same low value of A_{Py} is necessary to achieve the satisfactory agreement for the magnetoresistance hysteresis loops (see Sec. III).

The experimentally observed jump of frequency as a function of current is also seen in the simulated $f(I)$ curve for $A_{\mathrm{Py}} = 0.6 \times 10^{-6}$ erg/cm, albeit for a slightly different reduced current strength I/I_{cr}. As discussed in our Ref. 39, such a jump is due to transition between modes with different spatial localization patterns and as such should be sensitive to shape imperfections of the active layer. For this reason, we cannot expect the exact agreement of the simulated and measured frequencies for the jump locations.

The critical current and the current polarization. Our simulations show that the product of the critical current I_{cr} and the spin polarization of the current P is $P \cdot I_{\mathrm{cr}} \approx 0.055$ mA. Substitution of the experimental value of the threshold current $I_{\mathrm{cr}} \approx 1.9$ mA into this product results in the spin polarization $P \approx 0.03$. This polarization value is very low compared to typical values $P \sim 0.2$–0.4 calculated theoretically using quantum-mechanical models (see Ref. 3 and references therein) and estimated experimentally from critical currents measured for other systems. The reason for the low current polarization degree is not clear, but it might result from current spreading in the Cu spacer because the area of the spacer exceeds that of the CoFe nanomagnet (see Fig. 1 and Ref. 30). The low value of the current polarization is in agreement with the unusually high absolute value of the critical current density j_{cr} observed for the system under study. Substitution of $I_{\mathrm{cr}} \approx 1.9$ mA and the nominal lateral size of the CoFe nanoelement 50×50 nm^2 leads to the value $j_{\mathrm{cr}} = 7.6 \times 10^{11}$ A/m^2, which significantly exceeds j_{cr} observed in Py/Cu/Py (Ref. 39) and Co/Cu/Co trilayers.[5]

The estimated current polarization increases if we assume the conductivity of CoFe to decrease near the CoFe

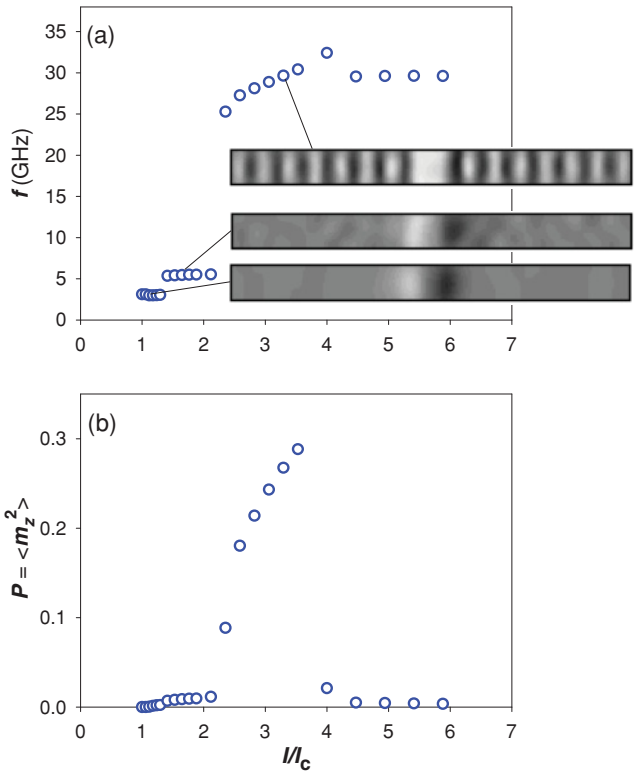

FIG. 9. (Color online) Py nanowire auto-oscillation modes for out-of-plane field $H_{perp} = 10$ kOe. Dependences of the oscillation frequency (a) and oscillation power (b) on the reduced current I/I_c. Gray-scale snapshots of the m_x component clearly show that oscillations after the second frequency jump correspond to a spin-wave mode propagating along the nanowire.

nanomagnet edges. This spatial dependence of the conductivity can result from partial oxidation or ion mill damage of the CoFe nanoelement edges during the sample preparation. We find that if the current flows mainly through the CoFe central region, the product $P{\cdot}I_{cr}$ increases, leading to higher values of P. Assuming that the current density is described by $j(x) \sim 1 - \exp(-x^2/2d^2)$, where x denotes the distance to the nearest edge, the product $P{\cdot}I_{cr}$ increases by a factor of 2 compared to the homogeneous current distribution.

The upper critical current (switching current). The current I_{sw}, at which magnetization switches from the steady-state oscillations to the 90° state [Fig. 4(b)] strongly depends on the magnetic material parameters. However, for all material parameters studied here, I_{sw} is much higher than that found experimentally. Whereas the measured upper critical current is $1.5{\cdot}I_{cr}$, the simulated I_{sw} is $(3–5){\cdot}I_{cr}$. The most probable reason for this discrepancy is that thermal fluctuations are neglected in our simulations. Thermal fluctuations present in the experiment should assist the transition to the 90° state.

To better understand stability of the 90° state, we performed simulations starting from *large* current values, gradually decreasing the current to zero. For this simulation protocol, the steady-state magnetization oscillations have not been observed for any current density. When the large spin torque corresponding to a large current density was turned on, the stable 90° state shown in Fig. 4(b) was quickly achieved. As we decreased the current, the system remained in the 90° state and magnetization auto-oscillations were not observed for any current values down to $I = 0$. This means that for the external field $H_x = 500$ Oe used in our simulations, the 90° state is metastable even in the absence of the spin torque. We have also verified the stability of the 90° state by simply minimizing the energy starting from this state. The 90° state is metastable due to the combined action of (i) the magnetodipolar interaction between the CoFe nanomagnet and the Py nanowire, and (ii) the in-plane shape anisotropy of the CoFe nanomagnet. Hence we conclude that the 90° state is separated by an energy barrier from the initial equilibrium state and from the dynamic state of auto-oscillations. This means that I_{sw} cannot be accurately determined by simulations performed at $T = 0$, because the transition to the 90° state takes place when magnetization overcomes the energy barrier due to thermal fluctuations. This finding is in very good agreement with the experiment. In the experiment, we observed that for the largest value of the current for which the auto-oscillations have been detected, the system could spend several minutes in the oscillating state and then irreversibly switch into a static state. Such a behavior is expected for a system where a relatively high energy barrier for the transition to the 90° state is present. At higher currents, the switching into a static state seen in the experiment was almost instantaneous.

Oscillation power. The largest disagreement between the simulations and the experiment is the dependence of the oscillation power on current. In Fig. 5(b), we display the averaged oscillation amplitude (computed as the maximal angle between the Py and CoFe magnetization averaged over the vertical stacks of discretization cells) deduced from the oscillation power. This figure shows that even for the Py exchange constant $A_{Py} = 0.65 \times 10^{-6}$ erg/cm, which provides a good agreement with the experimental oscillation frequency, the simulated power grows much slower with the current than the experimentally measured power. We verified that this discrepancy cannot be attributed to the higher conductivity of the central region of the CoFe square discussed above. Although the current confinement increases the value of the current polarization, the dependence of power on the reduced current $p(I/I_{cr})$ remains nearly the same.

E. Prospects for generating a propagating mode of auto-oscillations

Our simulations clearly show that the auto-oscillatory modes excited in our nanowire geometry for the in-plane magnetic-field configuration are strongly localized. Therefore this configuration is not suitable for phase locking of multiple ST nano-oscillators via spin waves propagating in the Py nanowire. To find a propagating mode in the geometry under study, we performed micromagnetic simulations for several other magnetic-field configurations. Since the main reason for the mode localization is the stray field of the CoFe nanomagnet, we focused on ST-induced magnetization auto-oscillations in strong out-of-plane fields. In this geometry, the influence of the CoFe stray field on spin waves in the Py layer is small.

Indeed, for the out-of-plane field geometry, our simulations show a rich mode structure with several transitions between different nonlinear modes with increasing current. In Fig. 9, we present a typical example of the system behavior in a

strong out-of-plane field $H_{perp} = 10$ kOe and magnetic material parameters $A_{Py} = 0.65 \times 10^{-6}$ erg/cm, $M_{Py} = 580$ emu/cm^3, $A_{CoFe} = 3 \times 10^{-6}$ erg/cm, and $M_{CoFe} = 1800$ emu/cm^3. For currents just above the onset of auto-oscillations, we observe a localized mode with nearly spatially uniform magnetization in the mode core. After the first frequency jump another localized mode with a more complicated spatial pattern of magnetization (but still localized well inside of the nanocontact area) emerges. Finally, the second frequency jump corresponds to the transition to a large-amplitude propagating spin-wave mode. Snapshots of the m_x component in the different dynamical regimes shown in Fig. 9 (a region of the system with lateral dimensions of 550×50 nm^2 surrounding the CoFe nanocontact is shown) confirm that the mode with the highest frequency is a propagating mode. Hence the out-of-plane field geometry is favorable for the generation of a propagating spin-wave mode in the 1D STNO system. The properties of this mode and perspectives of using this setup for synchronization of the STNOs on a nanowire will be discussed in a future publication.

V. CONCLUSIONS

We employed micromagnetic simulations to study magnetization dynamics induced by spin torque in a STNO system consisting of a CoFe nanomagnet current polarizer and a NiFe nanowire free layer. This system is of significant interest for studies of multiple STNO synchronization by spin waves propagating in a ferromagnetic nanowire.

Our simulations show that for the in-plane magnetic-field configuration, all auto-oscillatory modes in the NiFe nanowire are localized directly under the CoFe nanomagnet. This mode localization is induced by the large stray field of the CoFe nanomagnet. We find that the oscillation frequency of the localized modes sensitively depends on the NiFe and CoFe material parameters, especially on the exchange stiffness of the NiFe nanowire. The oscillation power of these modes depends nonmonotonically on the CoFe magnetization due to the resonant excitation of the CoFe nanomagnet edge modes by the oscillating magnetization of the NiFe nanowire.

The dependence of the frequency of the STNO modes on direct current bias given by our simulations is in good agreement with the experimental data for this system.[30] The simulations also successfully reproduce several other important features of the experimentally observed magnetization dynamics such as jumps of frequency with increasing current and metastable system behavior at high current densities. However, the dependence of the STNO power on the current bias given by the simulations is weaker than the experimentally measured dependence. Therefore quantitative description of magnetization dynamics induced by spin transfer torque remains a significant challenge.

Since the in-plane magnetic-field configuration yields localized auto-oscillatory modes unsuitable for synchronization of multiple STNOs via propagating spin waves, we studied magnetization dynamics in the out-of-plan field configuration. Our simulations show that an out-of-plane magnetic field sufficiently strong to saturate the NiFe magnetization perpendicular to the nanowire plane gives rise to a propagating current-driven auto-oscillatory mode in the NiFe nanowire. This propagating mode holds promise for the development of 1D phase-locked STNO arrays based on multiple nanocontacts to a ferromagnetic nanowire.

ACKNOWLEDGMENTS

The authors thank D. Mills, J. Katine, B. Gurney, P. Braganca, J. Childress, A. Slavin, and V. Tiberkevich for many useful discussions. This work was supported by NSF Grants No. DMR-0748810 and No. ECCS-0701458, by DARPA Grant No. HR0011-09-C-0114, and by the Nanoelectronics Research Initiative through the Western Institute of Nanoelectronics.

[1] J. C. Slonczewski, J. Magn. Magn. Mater. **159**, L1 (1996).
[2] L. Berger, Phys. Rev. B **54**, 9353 (1996).
[3] D. C. Ralph and M. D. Stiles, J. Magn. Magn. Mater. **320**, 1190 (2008).
[4] Y. Tserkovnyak, H. J. Skadsem, A. Brataas, and G. E. W. Bauer, Phys. Rev. B **74**, 144405 (2006).
[5] S. I. Kiselev, J. C. Sankey, I. N. Krivorotov, N. C. Emley, R. J. Schoelkopf, R. A. Buhrman, and D. C. Ralph, Nature (London) **425**, 380 (2003).
[6] W. H. Rippard, M. R. Pufall, S. Kaka, S. E. Russek, and T. J. Silva, Phys. Rev. Lett. **92**, 027201 (2004).
[7] M. Tsoi, A. G. M. Jansen, J. Bass, W. C. Chiang, M. Seck, V. Tsoi, and P. Wyder, Phys. Rev. Lett. **80**, 4281 (1998).
[8] T. J. Silva and W. H. Rippard, J. Magn. Magn. Mater. **320**, 1260 (2008).
[9] A. L. Chudnovskiy, J. Swiebodzinski, and A. Kamenev, Phys. Rev. Lett. **101**, 066601 (2008).
[10] Y. Zhou, J. Persson, S. Bonetti, and J. Åkerman, Appl. Phys. Lett. **92**, 092505 (2008).
[11] S. Kaka, M. R. Pufall, W. H. Rippard, T. J. Silva, S. E. Russek, and J. A. Katine, Nature (London) **437**, 389 (2005).
[12] F. B. Mancoff, N. D. Rizzo, B. N. Engel, and S. Tehrani, Nature (London) **437**, 393 (2005).
[13] A. Ruotolo, V. Cros, B. Georges, A. Dussaux, J. Grollier, C. Deranlot, R. Guillemet, K. Bouzehouane, S. Fusil, and A. Fert, Nat. Nanotechnol. **4**, 528 (2009).
[14] X. Chen and R. H. Victora, Phys. Rev. B **79**, 180402 (2009).
[15] R. Matsumoto, A. Fukushima, K. Yakushiji, S. Yakata, T. Nagahama, H. Kubota, T. Katayama, Y. Suzuki, K. Ando, S. Yuasa, B. Georges, V. Cros, J. Grollier, and A. Fert, Phys. Rev. B **80**, 174405 (2009).
[16] D. Houssameddine, U. Ebels, B. Dieny, K. Garello, J.-P. Michel, B. Delaet, B. Viala, M.-C. Cyrille, D. Mauri, and J. A. Katine, Phys. Rev. Lett. **102**, 257202 (2009).
[17] A. M. Deac, A. Fukushima, H. Kubota, H. Maehara, Y. Suzuki, S. Yuasa, Y. Nagamine, K. Tsunekawa, D. D. Djayaprawira, and N. Watanabe, Nature Phys. **4**, 803 (2008).
[18] T. Wada, T. Yamane, T. Seki, T. Nozaki, Y. Suzuki, H. Kubota, A. Fukushima, S. Yuasa, H. Maehara, Y. Nagamine, K. Tsunekawa, D. D. Djayaprawira, and N. Watanabe, Phys. Rev. B **81**, 104410 (2010).

[19]A. Slavin and V. Tiberkevich, IEEE Trans. Magn. **45**, 1875 (2009).
[20]V. S. Tiberkevich, A. N. Slavin, and J. V. Kim, Phys. Rev. B **78**, 092401 (2008).
[21]R. Bonin, C. Serpico, G. Bertotti, I. D. Mayergoyz, and M. d'Aquino, Eur. Phys. J. B **59**, 435 (2007).
[22]W. Chen, G. de Loubens, J.-M. L. Beaujour, J. Z. Sun, and A. D. Kent, Appl. Phys. Lett. **95**, 172513 (2009).
[23]S. Urazhdin, P. Tabor, V. Tiberkevich, and A. Slavin, Phys. Rev. Lett. **105**, 104101 (2010).
[24]Y. B. Bazaliy, Phys. Rev. B **76**, 140402 (2007).
[25]X. Cheng, C. T. Boone, J. Zhu, and I. N. Krivorotov, Phys. Rev. Lett. **105**, 047202 (2010).
[26]D. M. Apalkov and P. B. Visscher, Phys. Rev. B **72**, 180405(R) (2005).
[27]R. Lehndorff, D. E. Bürgler, S. Gliga, R. Hertel, P. Grünberg, C. M. Schneider, and Z. Celinski, Phys. Rev. B **80**, 054412 (2009).
[28]P. M. Braganca, B. A. Gurney, B. A. Wilson, J. A. Katine, S. Maat, and J. R. Childress, Nanotechnology **21**, 235202 (2010).
[29]M. A. Hoefer, T. J. Silva, and M. W. Keller, Phys. Rev. B **82**, 054432 (2010).
[30]C. Boone, J. A. Katine, J. R. Childress, J. Zhu, X. Cheng, and I. N. Krivorotov, Phys. Rev. B **79**, 140404 (2009).
[31]D. V. Berkov and N. L. Gorn, MicroMagus – package for micromagnetic simulations [http://www.micromagus.de].
[32]J. Xiao, A. Zangwill, and M. D. Stiles, Phys. Rev. B **70**, 172405 (2004).
[33]A. Slavin and V. Tiberkevich, Phys. Rev. Lett. **95**, 237201 (2005).
[34]Q. Mistral, M. van Kampen, G. Hrkac, J.-V. Kim, T. Devolder, P. Crozat, C. Chappert, L. Lagae, and T. Schrefl, Phys. Rev. Lett. **100**, 257201 (2008).
[35]S. Komineas, Phys. Rev. Lett. **99**, 117202 (2007).
[36]G. Finocchio, O. Ozatay, L. Torres, R. A. Buhrman, D. C. Ralph, and B. Azzerboni, Phys. Rev. B **78**, 174408 (2008).
[37]D. V. Berkov and N. L. Gorn, Phys. Rev. B **80**, 064409 (2009).
[38]C. Bayer, J. Jorzick, B. Hillebrands, S. O. Demokritov, R. Kouba, R. Bozinoski, A. N. Slavin, K. Guslienko, D. V. Berkov, N. L. Gorn, and M. P. Kostylev, Phys. Rev. B **72**, 064427 (2005).
[39]I. N. Krivorotov, D. V. Berkov, N. L. Gorn, N. C. Emley, J. C. Sankey, D. C. Ralph, and R. A. Buhrman, Phys. Rev. B **76**, 024418 (2007).
[40]A. Slavin and V. Tiberkevich, IEEE Trans. Magn. **44**, 1916 (2008).
[41]A. Helmer, S. Cornelissen, T. Devolder, J.-V. Kim, W. van Roy, L. Lagae, and C. Chappert, Phys. Rev. B **81**, 094416 (2010).
[42]X. Liu, R. Sootyakumar, C. J. Gutierrez, and G. A. Prinz, J. Appl. Phys. **75**, 7021 (1994).